Dual-Band Dual-Polarized Array Based on Electromagnetic Transparent Antenna for Vehicle-Mounted Base Station Systems

Xuekang Liu, Benito Sanz-Izquierdo, *Senior Member, IEEE*, Steven Gao, *Fellow, IEEE*, Qi Luo, *Senior Member, IEEE,* Lu Zhang, Lehu Wen, *Senior Member*, IEEE, Xue-Xia Yang, *Senior Member, IEEE,* and Lei Wang

***Abstract*—This paper introduces a novel ±45° shared-aperture, dual-band, dual-polarized interleaved array for vehicle-mounted base station systems. The array integrates a lower band (LB) antenna with four higher band (HB) antennas. To address the issue of cross-band scattering and its impact on higher band performance, we employ an innovative method that involves reducing the aperture size and incorporating lumped or distributed inductors. These inductors function as frequency-selective structures, permitting low-frequency currents to pass while blocking high-frequency currents. Consequently, at high frequencies, these inductors act as open circuits, making the low-frequency antenna radiator resemble multiple discontinuous small metal strips. This approach achieves an electromagnetic transparent (EMT) bandwidth of over 82.9%, making it highly suitable for mobile base station applications. By integrating this low-scattering LB antenna with four bandwidth-optimized cross dipoles, we achieve a dual-band interleaved array. The measured results confirm that the dual-band array operates effectively within the 0.85-0.98 GHz and 1.4-2.7 GHz frequency ranges, maintaining stable radiation performance. The superior performance of this design makes it an ideal choice for vehicle-based base stations.**

***Index Terms*—Array antenna, cross-band scattering, dual-polarized antenna, vehicle to everything, Vehicle-Mounted Base Station.**

 This research received partial funding from the Engineering and Physical Sciences Research Council (EPSRC) under Grant EP/Y003144/2, Huawei Technologies Ltd, and the Research Grants Council of Hong Kong under Grants GRF 14210623 and AoE/E-101/23-N. (Corresponding author: *Xuekang Liu*)

Xuekang Liu and Lei Wang are with the School of Engineering, Lancaster University, Lancaster, LA1 4YW, U.K. (e-mail: xuekangliu@ieee.org, lei.wang@lancaster.ac.uk).

Benito Sanz-Izquierdo is with the School of Engineering, University of Kent, Canterbury CT2 7NT, U.K. (e-mail: b.sanz@kent.ac.uk)

Steven Gao is with the Dept of Electronic Engineering, Chinese University of Hong Kong. (e-mail: scgao@ee.cuhk.edu.hk)

Qi. Luo is with the School of Physics, Engineering and Computer Science, University of Hertfordshire, Hatfield AL10 9AB, U.K. (e-mail: q.luo2@herts.ac.uk)

Lu Zhang is with the Faculty of Science and Engineering, Swansea University, Swansea, SA1 8EN, U.K. (e-mail: lu.zhang@swansea.ac.uk)

Lehu Wen is with the Department of Electronic and Electrical Engineering, Brunel University London, UB8 3PH, Uxbridge, U.K. (e-mail: lehuwen@ieee.org)

Xue-Xia Yang is with the School of Communication and Information Engineering, Shanghai University, Shanghai 200444, China. (e-mail: yang.xx@shu.edu.cn)

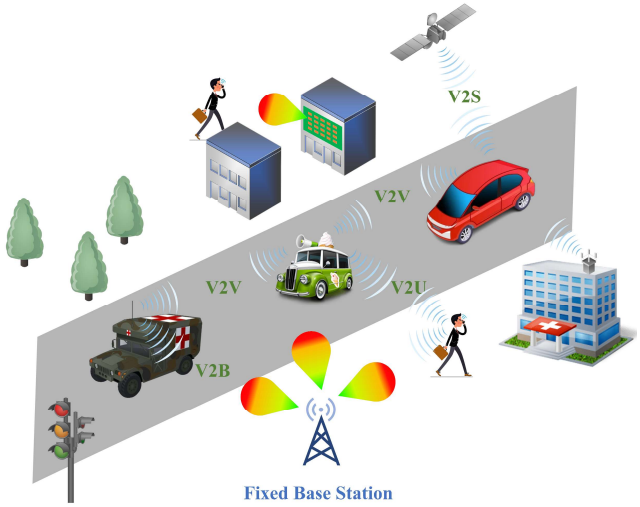

Fig. 1. Schematic diagram of a typical urban communication network.

I. INTRODUCTION

VEHICLE to everything (V2X) communication [1] represents a significant evolution in how vehicles interact with their environment. As shown in Fig. 1, V2X technology unifies various communication channels, creating an extensive network that connects vehicles not only with each other (V2V) but also with broader infrastructure systems. This enables real-time data exchange between vehicles and base stations (V2B), vehicles and users (V2U), and vehicles and satellites (V2S).

In this ecosystem, fixed base stations and vehicle-mounted base stations are essential components, serving as central nodes that link terminal devices to broader networks. Fixed base stations [2] ensure reliable and stable coverage across urban, suburban, and rural regions. They play a crucial role in maintaining the smooth operation of cellular networks, supporting services like voice, data, and multimedia. These stations are strategically located in areas with high communication demand, such as cities, towns, highways, and densely populated zones. Installing them requires significant infrastructure, including power supplies, backhaul connections, and site security.

In contrast, vehicle-mounted base stations [3], [4], offer

Fig. 2. Application scenarios of the vehicle-mounted base stations.

flexible and temporary coverage, particularly useful in areas where fixed base stations are not available or during emergency situations. As shown in Fig.2, these mobile units can be quickly deployed to provide network services in various scenarios, such as rural area coverage, large events like music festivals, medical missions, and disaster relief operations. Unlike fixed base stations, vehicle-mounted base stations do not require extensive infrastructure and can be moved as needed, offering a versatile solution for maintaining connectivity in dynamic environments. Their mobility makes them invaluable in ensuring continuous communication, even in challenging or rapidly changing situations.

To support these dynamic applications, vehicle-mounted base stations commonly utilize dual-polarized antennas [5], [6], [7], [8], [9], [10]. These antennas, capable of simultaneously receiving and transmitting two orthogonal polarization signals, enhance spectral efficiency and signal quality, which is crucial for robust communication in challenging conditions. However, as the demand for V2X services grows, along with the need to support multiple frequency bands used by user terminals, more antennas are being placed within the limited space of vehicle-mounted base stations [11]. This shift towards more compact and densely packed designs has introduced challenges, particularly concerning in-band/cross-band mutual coupling between antennas, which can degrade base station performance [12], [13]. Addressing these challenges is essential to ensure that vehicle-mounted base stations maintain the high levels of isolation required for efficient operation across multiple frequency bands, thereby continuing to support the growing demands of the V2X ecosystem.

In-band mutual coupling can be effectively suppressed by utilizing decoupling ground [14], planar metamaterial structure (PMS) and array-antenna decoupling surface (ADS) [15], and metallic strips [16]. However, the cross-band mutual coupling is still a challenge. The use of filtering antennas [17], [18], [19] emerged as a viable solution to enhance port isolation of base station antennas. Nevertheless, in a dual-band shared-aperture array, the antennas operating at the lower frequency band (LB antennas) are typically positioned above

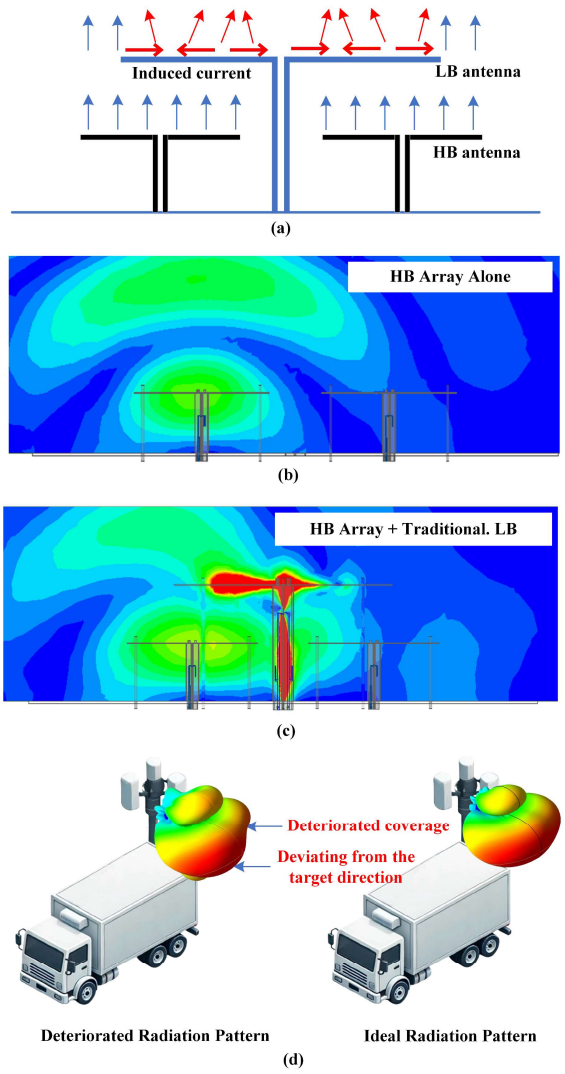

Fig. 3. (a) Schematic diagram of the cross-band scattering, (b)E-field distribution of HB array alone, (c) E-field distribution of the HB array with unaltered LB antenna, and (d) influence of cross-band scattering on vehicle-mounted base stations.

those operating at the higher frequency band (HB antennas). When the HB antennas are excited, they radiate electromagnetic (EM) waves into free space. These radiated waves induce currents in the radiators of the LB antennas, which in turn generate secondary EM waves that radiate into free space. A phenomenon known as cross-band scattering [20]. This alteration leads to unexpected changes in the gains and radiation patterns of the HB array. Addressing this challenge is crucial for the continued advancement and reliability of vehicle-mounted base stations.

In recent years, several innovative methods were developed to solve this problem. Frequency selective surfaces are used in [21] and [22] to reduce the cross-band scattering. These frequency selective surfaces can selectively pass or block electromagnetic waves in different frequency bands. Therefore, by rationally arranging the relative positions of LB and higher band (HB) antennas, physical isolation between them can be achieved, thereby reducing cross-band scattering.

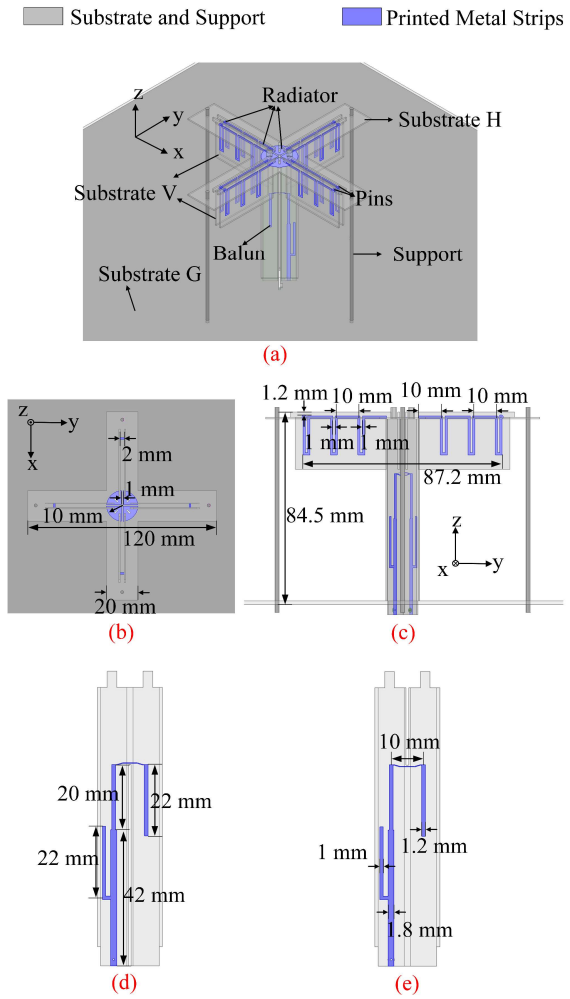

Fig. 4. The geometry of the low-scattering LB antenna. (a) Overall view, (b) Top view, (c) Side view, and (d), (e) Baluns.

However, this will greatly increase the complexity of the base station. Chokes [23], [24] and meta surface [25], [26] can also be utilized to mitigate the cross-band scattering in dual-/multi-band arrays. However, the electromagnetic transparent (EMT) bandwidths of the LB antennas in these designs are relatively narrow. To obtain a wider EMT bandwidth, several EMT antennas are realized by using slot loaded radiator [27], open-end branches [28], [29], and multiple folded dipole antenna [30]. Although the EMT bandwidths of these designs are wider than 30%, it still falls short for the needs of today's highly integrated vehicle-mounted base stations.

We present an innovative approach to reduce cross-band scattering in dual-band arrays and applied it in the design of dual-band vehicle-mounted base stations, thereby enhancing the performance of mobile base station-centric wireless communication networks. By minimizing the antenna aperture and incorporating lumped and distributed inductors, we have developed an LB antenna with an EMT bandwidth exceeding 82.9%. This represents the widest EMT bandwidth compared to published articles. All simulated results presented in this paper were obtained using ANSYS HFSS (High-Frequency Structure Simulator).

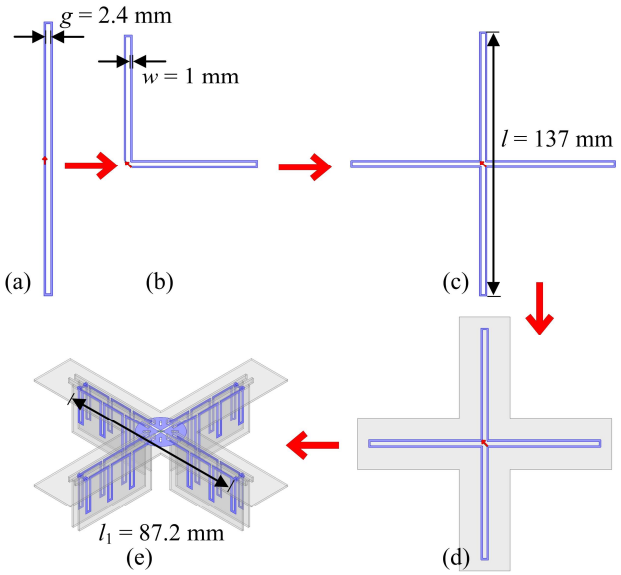

Fig. 5. Evolution of the radiator. Configurations of (a) Rad.1, (b) Rad.2, (c) Rad.3, (d) Rad.4, and (e) Rad.5.

II. Miniaturized Dual-Polarized LB Antenna

The design of the low-scattering LB antenna from multiple angles are given in Fig. 4. The horizontal parts of the radiator are printed on substrate H, while the vertical parts are printed on substrate V. To achieve ±45° polarizations, two vertically printed baluns are connected to the antenna radiator. Additionally, Fig. 4 also provides the precise sizes of both the radiator and the baluns. The design uses Rogers Ro4003™ substrates, known for their relative permittivity of 3.55 and dielectric loss tangent of 0.0027. Substrate G has a thickness of 1.524 mm, whereas substrates H and V each have a thickness of 0.813 mm. A thicker substrate was selected to prevent any deformation that could occur with larger sizes, which might otherwise impair the antenna's performance.

Fig. 5 outlines the step-by-step development of the antenna's radiator, showing how the design evolves from its initial concept (single polarized radiator) to the final version (miniaturized dual-polarized radiator). The process starts with a simple folded dipole antenna, named Rad.1. This basic model is then modified through bending to create Rad.2. The evolution continues by combining two Rad.2 units, resulting in Rad.3. To make the antenna easier to manufacture, the next step involves adding a substrate to the design, evolving it into Rad.4. The final adjustment in the design process is bending Rad.4 vertically, creating Rad.5. This version is more compact but still retains the performance of its predecessors, addressing the need for an antenna that performs well while saving space. It's important to highlight that the radiator's aperture size can be significantly decreased by 59.5%, bringing it down to 40.5% of its original size.

To determine the operating frequency band of the design, the input impedance of Rad.1 and reflection coefficient can be used as a starting point. The input impedance Z_{in} of the printed dipole antenna can be calculated by using [31]:

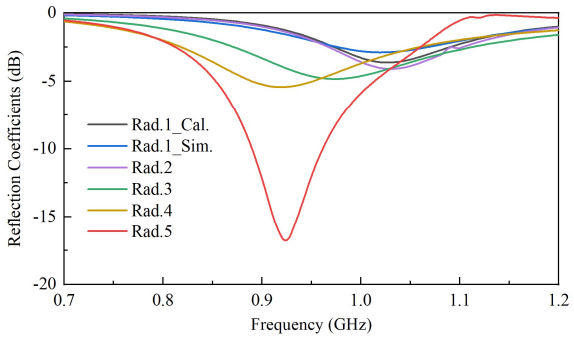

Fig. 6. Calculated and simulated reflection coefficients of the radiators.

$$Z_{in} = \frac{2(1+a)^2 Z_d Z_t}{(1+a)^2 Z_d + 2Z_t} \quad (1)$$

where Z_t and Z_d are the input impedances of the transmission line mode and dipole mode. $(1+a)^2$ is the impedance step-up ratio [32]. In this case, given that the printed strips maintain a consistent width, the value of a is set to 1. Thus, equation (1) can be reduced to:

$$Z_{in} = \frac{4Z_d Z_t}{2Z_d + Z_t} \quad (2)$$

The input impedance of the transmission line mode (Z_t) can be represented as:

$$Z_t = jZ_0 \tan(k \cdot \frac{l}{2}) \quad (3)$$

k is the propagation constant; l is the length of the folded dipole antenna. Z_0 is the characteristic impedance of a coplanar strip transmission line. It can be calculated as:

$$Z_0 = 120\pi \frac{K(x)}{K'(x)} \quad (4)$$

In (6), $K(x)$ is the complete elliptic function of the first kind. It has the following characteristics:

$$K'(x) = K(x') \quad (5)$$

$$x^2 + x'^2 = 1 \quad (6)$$

Where x is related to the size of the folded dipole antenna:

$$x = \frac{g}{g + 2W} \quad (7)$$

The input impedance of the dipole mode can be substituting

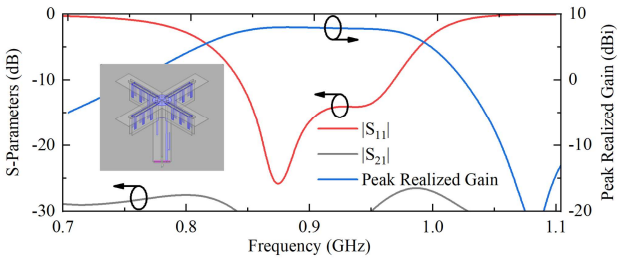

Fig. 7. Simulated peak realized gain and S-parameters of the proposed LB antenna.

the equivalent radius (a_e) into the following equations [33]:

$$Z_d = \frac{R_d + jX_d}{sin^2(kl)} \quad (8)$$

where R_d and X_d can be obtained by using the equations in [33].

With the help of the commercial software MATLAB, we obtained the calculated reflection coefficient for the folded dipole based on the input impedance derived from the above method, as illustrated in Fig. 6. When this is compared to the simulated result derived from another commercial software, ANSYS HFSS, it becomes evident that the calculated and simulated results are almost identical. Hence, the equations allow for the swift identification of printed folded dipole's resonant frequency without using the full wave electromagnetic simulation software.

By bending the folded dipole in its middle, a bended folded dipole (Rad.2) can be realized. It can be clearly seen in Fig. 6 that bending has little effect on the S parameter of folded dipole. Then, by combining two identical bended folded dipoles together. A four-legged loaded element (Rad.3) can be realized. Fig. 6 demonstrates that the introduction of the substrate causes a slight shift in the resonant frequency of the four-legged loaded element towards the lower frequency band. Finally, to reduce the aperture size of the radiator, it was bent longitudinally to form Rad.5. The Rad.5 has not only a much smaller aperture size (40% of Rad.4), but also a better impedance bandwidth.

Rad.5 is a balanced structure, while coaxial cables are typically unbalanced. Therefore, a balun is required to connect Rad.5 to the cables, enabling the conversion between balanced and unbalanced configurations. By adjusting the widths and lengths of the microstrip and coupled microstrip lines, the input impedance of the radiator can be transformed to 50 Ω. The incorporation of the L-shaped structure adds flexibility to the balun design, simplifying the impedance transformation process.

Fig. 7 illustrates the $|S_{11}|$, $|S_{21}|$, and peak realized gain of the final LB antenna. The antenna operates within the 0.84-0.97 GHz frequency range, achieving an average peak realized gain of 7.9 dBi. The simulated isolation of the proposed LB antenna exceeds 27.24 dB across the operating frequency range, making it a good candidate for base station applications.

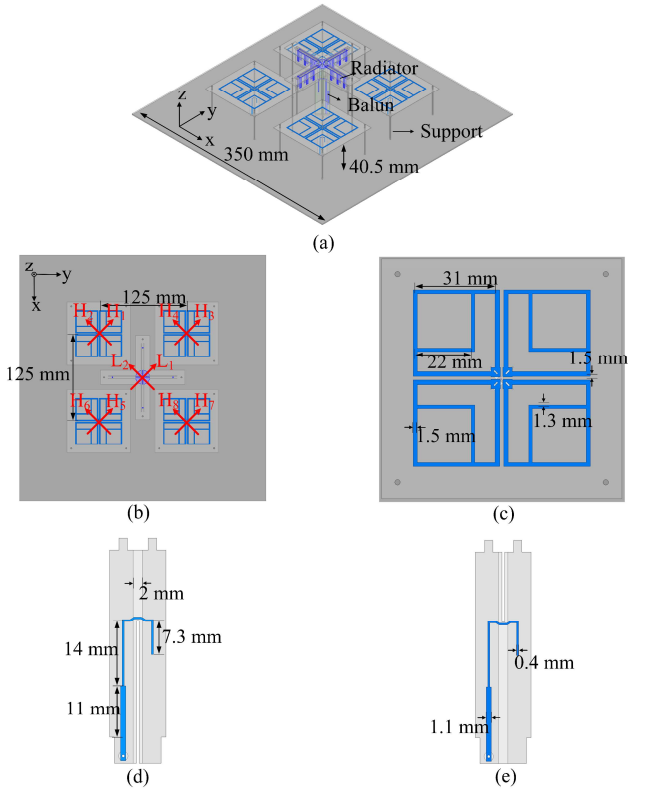

Fig. 8. The geometry of the proposed dual-band dual-polarized array. (a) Overall view, (b) top view, (c)top view of HB element, and (d), (e) baluns of HB element.

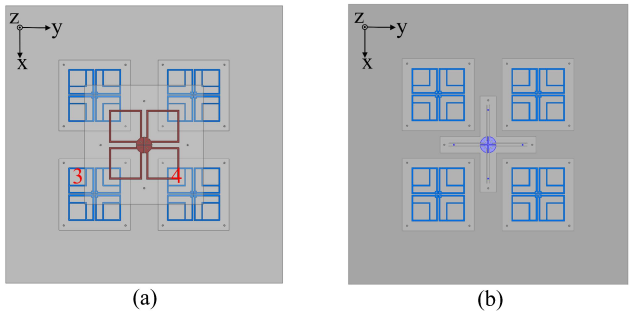

Fig. 9. Comparison of the LB antenna in (a) the reference array and (b) the proposed array.

III. Suppression of Cross-Band Scattering

The configuration of the proposed dual-band dual-polarized array is shown in Fig. 8. It includes one LB element and four HB elements. The array features a total of 10 input ports, with 8 designated for activating HB antennas and 2 for the LB antenna. The operating principle of the HB antenna has been detailed in [34]. In this design, cross strips and open-end branches are removed since there is no need for radiation suppression in the higher frequency band. The detailed dimensions of the HB element are provided in Fig. 8(c)-(e).To better demonstrate the advantages of the proposed design, a reference dual-band dual-polarized array is simulated by using ANSYS HFSS. It is worth noting that the configuration of the reference array is nearly identical with the proposed array except the structure of the LB antenna.

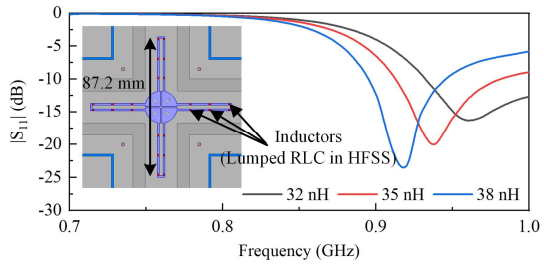

Fig. 10. Simulated $|S_{11}|$ of the miniaturized lumped inductor-loaded LB antenna under different inductor values.

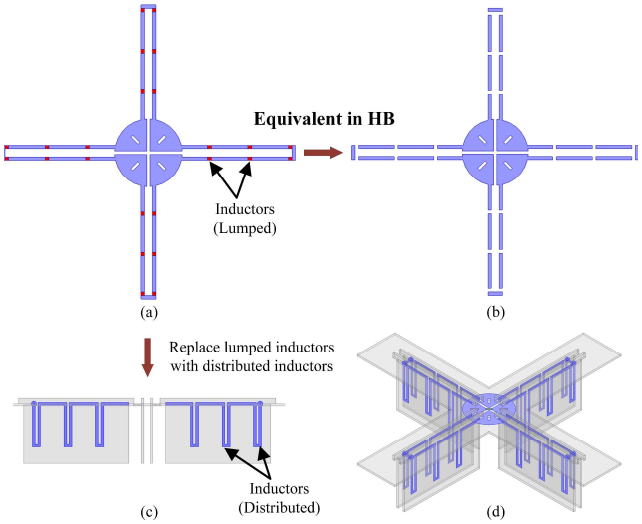

Fig. 11. (a) The radiator with lumped inductors, (b) the equivalent structure of the lumped inductor-loaded LB radiator in the HB, (c) side view of the radiator with distributed inductors, and (d) 3D view of the radiator with distributed inductors.

The low-scattering characteristics of the proposed LB antenna is achieved through a two-step method. First, the size of the LB radiator is reduced to minimize the metal area above the HB array. As shown in Fig. 9, the radiator of the proposed LB antenna is concentrated in the central cross area, with no metal directly above the HB antennas. The entire radiator can be seen as a folded loop, effectively reducing cross-band scattering.

The second step involves introducing lumped/distributed inductors. Starting with Rad. 4 in Fig. 5, to further mitigate cross-band scattering, the aperture size has been reduced, and several lumped inductors have been added, as illustrated in Fig. 10. These inductors perform two main functions. First, they help in tuning the LB antenna's resonant frequency, as shown by the simulated $|S_{11}|$ under various inductance values in Fig. 10. As observed, adjusting the inductance values shifts the resonant frequency of the antenna towards the lower frequency band, without changing the antenna size.

Second, the inductors act as filters, allowing low-frequency currents to pass with relatively small impedance while blocking high-frequency currents. This behavior is due to the inductive reactance, which increases with frequency, thus enabling low-frequency signals to pass and significantly impeding high-frequency signals. Consequently, as shown in

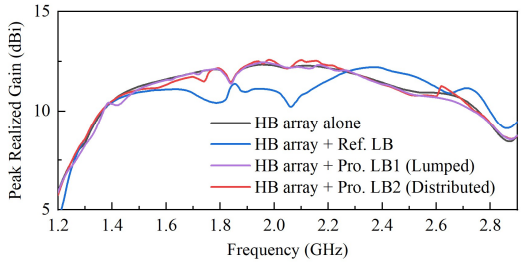

Fig. 12. Simulated peak realized gains of the HB array in different configurations.

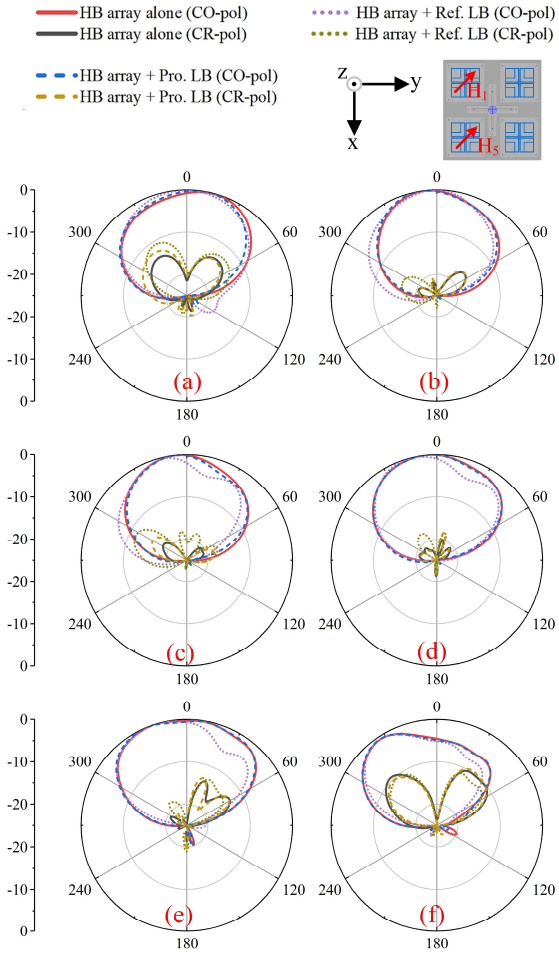

Fig. 13. Simulated normalized radiation patterns in horizontal planes (yoz) of the HB array (ports 1 and 5 are excited) in different configurations at (a) 1.2 GHz, (b) 1.7 GHz, (c) 2.0 GHz, (d) 2.3 GHz, (e) 2.6 GHz, and (f) 2.9 GHz.

Fig. 11, the radiator can be modeled as many small metal strips, each much smaller than ½ $\lambda_{2.7\ GHz}$ (free space wavelength at the highest frequency of HB), resulting in low cross-band scattering.

Benefit from the impedance transformation characteristics of transmission lines, a section of short-circuit transmission lines can be equivalent to an inductor when its length is shorter than ¼ λ [35]. Thus, the lumped inductors can be replaced by short-circuit transmission lines with certain lengths, as shown in Fig. 11 (c) and (d). By replacing the lump inductors in Fig. 11(a) with short-circuit transmission

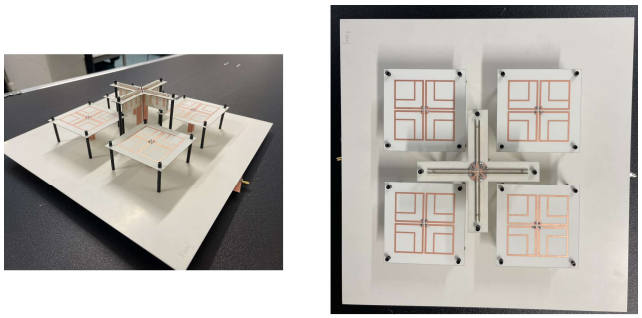

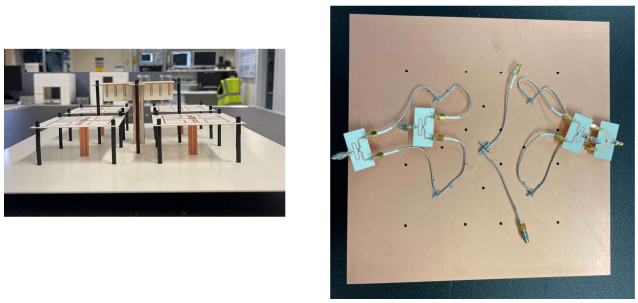

Fig. 14. Photos of the prototype. (a) Overall view, (b) top view, (c) side view, and (d) back view.

lines and connecting the radiator to optimized baluns, the proposed LB antenna (with distributed inductors) can be obtained.

To demonstrate the effectiveness of the proposed new antenna and method, simulated gains and radiation patterns of the HB array alone, with traditional dual-polarized LB antenna, and with the proposed miniaturized dual-polarized LB antennas are compared in Fig. 12 and 13. It is clear that the proposed LB antennas has minimal effect on the HB array's radiation performance, which is vital for dual-/multiband interleaved array designs.

The simulated peak realized gains are shown in Fig. 12. As observed, the reference LB antenna significantly affects the gain of the HB array. The maximum difference in peak realized gain for the HB array, with and without reference LB antenna, is 1.95 dBi. This results in severe impairment of mobile base station performance in this frequency band. The difference in peak realized gain for the HB array, with and without the proposed distributed inductor-loaded LB antenna, is less than 0.5 dBi, which is significantly smaller than the 1.95 dBi difference typically observed in traditional dual-band arrays. Additionally, the difference in peak realized gain for the HB array, with and without the lumped inductor-loaded LB antenna, is even smaller at less than 0.45 dBi, indicating slightly better performance than the distributed design. However, as the distributed inductor-loaded design is easier to fabricate and the performance difference is minimal, we selected it for fabrication.

Fig. 13 compares the normalized radiation patterns for the HB array in various configurations: the HB array alone, the HB array with the reference LB antenna, and the HB array

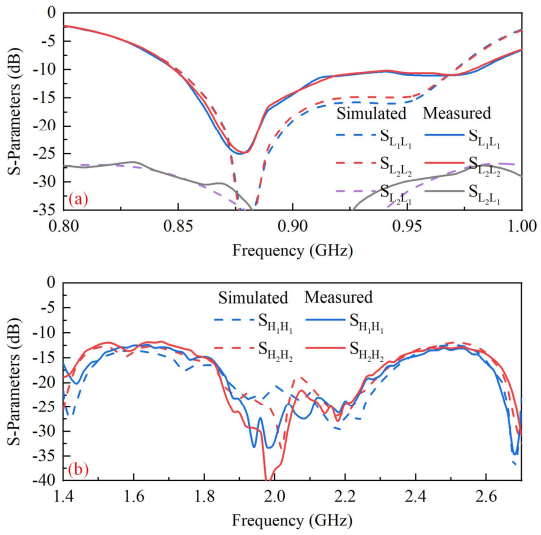

Fig. 15. S-parameters of the dual-band array.

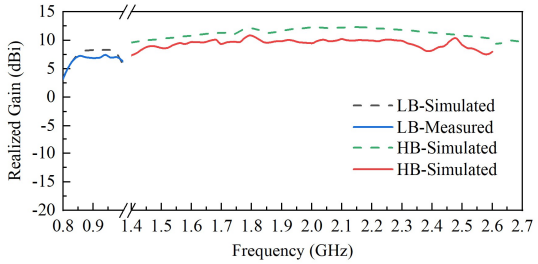

Fig. 16. Boresight realized gains of the proposed dual-band array.

with the proposed distributed LB antenna. Due to the symmetry of the array, only ports 1 and 5 are excited as examples. It is evident that the induced current on the radiator of the reference LB antenna emits unwanted electromagnetic waves within the HB antennas' operating band, causing significant distortion in the HB antenna's radiation pattern. The change in the radiation patterns can lead to poor directivity and reduced controllability in the mobile base station antenna. This, in turn, affects the communication quality of mobile base station-centered wireless networks, ultimately diminishing users' experience with the infrastructure. Fig. 13 also illustrate that the proposed LB antenna with distributed inductors have very little influence on the radiation patterns of the HB array. Thus, this antenna achieve coverage in the lower frequency band while maintaining low cross-band scattering in the higher frequency band. It is noteworthy that while the impedance bandwidth of the HB array proposed in this paper does not fully cover the 1.2–2.9 GHz range, Figs. 12 and 13 clearly demonstrate that the EMT band of the proposed LB antenna successfully covers the 1.2–2.9 GHz range. The distortion observed in the radiation patterns in Fig. 13(f) is caused by the imbalance of the baluns at 2.9 GHz. At this frequency, the baluns fail to effectively convert the unbalanced feed into a balanced feed, resulting in an uneven current distribution between the two arms of the dipoles and, consequently, distortion in the radiation pattern.

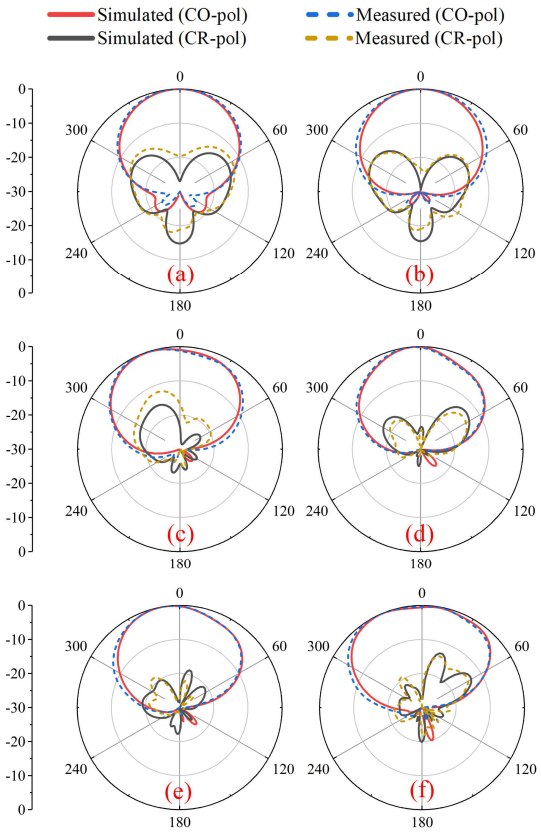

Fig. 17. Normalized radiation patterns of the LB array at (a) 0.85 GHz, (b) 0.95 GHz, and HB array at (c) 1.4 GHz, (d) 1.8 GHz, (e) 2.2 GHz, and (f) 2.6 GHz.

IV. Measured Results and Discussion

To demonstrate the design concept, a prototype of this dual-band array was fabricated and tested. The photos of the prototype are shown in Fig. 14. The power dividers connected to the HB antennas are used to measure the radiation patterns of the HB array. The measured results show a close match with the simulated ones. The discrepancies observed were primarily due to fabrication and measurement inaccuracies.

Fig. 15 depicts the operational frequency range of the LB antenna, spanning from 0.85 GHz to 0.98 GHz, while the HB antenna covers the range from 1.4 GHz to 2.7 GHz. The measured isolations of the LB antenna in the dual-band array align closely with the simulated results, with values exceeding 27 dB throughout the operating frequency band. Fig. 16 presents the boresight realized gains for both LB and HB modes of the dual-band array. The LB antenna achieved an average measured realized gain of 7.1 dBi within its operational range. The HB array, when excited at ports H_1 and H_5, demonstrated an average measured realized gain of 9.1 dBi within its frequency band.

The radiation performance of the dual-band array were measured at the University of Kent's antenna lab. Fig. 17(a) and (b) shows the radiation pattern of the LB antenna at 0.85 GHz and 0.95 GHz, including both measured and simulated results. The results indicate stable radiation patterns with

TABLE I
COMPARISON OF THE DUAL-BAND DUAL-POLARIZED ARRAYS

Ref.	Configuration	Gain Comparison	EMT Bandwidth (GHz)	LB Bandwidth (GHz)	FR	Complexity	Methods	HB Spacing (λ_{HL})
[20]	Interleaved	Yes, ±1.4 dBi	45% (1.71-2.71)	40.8% (0.66-0.997)	2.67	High	Metasurface cloak	0.64 × 0.98
[22]	2×2 HB above LB	No	33% (3.5-4.9)	32.7% (0.69-0.96)	5.09	High	FSS	0.73 × 0.73
[24]	Interleaved	No	11.4% (3.3-3.7)	31.6% (1.65-2.27)	1.76	Moderate	Chokes	0.76 × 0.99
[27]	Interleaved	No	34% (1.7-2.4)	32.7% (0.69-0.96)	2.48	High	Slots	0.71 × 0.71
[28]	Interleaved	No	46% (1.7-2.7)	32.7% (0.69-0.96)	2.7	Simple	Open-end Branches	/
[36]	Interleaved	Yes, ±0.5 dBi	14% (3.3-3.8)	24% (1.71-2.17)	1.8	Moderate	Shorted Patches	0.57 × 0.86
[37]	LB stacked on a HB	Yes, ±0.4 dBi	14% (3.3-3.8)	16% (2.3-2.7)	1.42	Simple	FSS Radiator	/
[38]	LB stacked on a HB	No	66.7% (1.36-2.72)	18.2% (0.80-0.96)	2.32	High	Helical Filters	/
Pro.	**Interleaved**	**Yes, ±0.5 dBi**	**82.9% (1.2-2.9)**	**14.2% (0.85-0.98)**	**2.27**	**Moderate**	**Distributed Inductors**	0.58 × 0.58

* Gain Comparison refers to the evaluation of the gain between the HB array alone and the array with the proposed design. λ_{HL}, is the wavelength at the lowest operating frequency in free space of higher band. EMT represents electromagnetic transparent, FR means frequency ratio.

HPBWs of approximately 64° throughout its operational band. Fig. 17(c)-(f) illustrates the normalized radiation patterns of the HB array, where the measured data closely match the simulations. These simulations were conducted using Ansys HFSS software:

$$E_{+45^\circ}(\theta) = \frac{E_\varphi(\theta) * cos45^\circ + E_\theta(\theta) * cos45^\circ}{max(E_{total})} \quad (9)$$

$$E_{-45^\circ}(\theta) = \frac{E_\theta(\theta) * cos45^\circ - E_\varphi(\theta) * cos45^\circ}{max(E_{total})} \quad (10)$$

Table I provides a detailed comparison of the proposed dual-band array with several other designs previously presented. The design in [20] achieves a relatively wide EMT bandwidth when the impedance bandwidth itself is also relatively wide. However, its in-band characteristics are unstable, with a mutation point (914 MHz) in the GSM 900 and LTE 900 bands. The designs in [22], [24], [27], [28] achieve wider impedance bandwidths, but their EMT bandwidths are much narrower than the design proposed in this paper. None of these designs can cover the widely used 1.4–2.7 GHz frequency band for base stations, and they did not provide a gain comparison of the HB antenna/array under different conditions to do a fair comparison. Moreover, the designs in [22] and [27] are more complex, making them harder to design and fabricate. [36] and [37] include a gain comparison of HB antenna/array under different conditions and show that the LB antenna impacts the HB antenna/array's gain by less than 0.5 dBi, similar to the design in this paper. However, their EMT bandwidth is only one-sixth of the bandwidth achieved by the proposed design. [38] presents an EMT antenna with performance similar to the design in this paper. However, its array layout (with the LB antenna stacked on the HB antenna) differs from this design, and its EMT bandwidth is narrower. The paper did not provide a gain comparison of the high-frequency antenna under different conditions, and its three-dimensional spiral structure is more complex and harder to fabricate compared to this design.

V. CONCLUSION

This paper introduces a novel shared-aperture dual-band dual-polarized interleaved array that integrates a low-scattering LB antenna with four bandwidth-enhanced tightly coupled cross-dipoles. The operational principles, including impedance and scattering characteristics of the LB antenna, were rigorously analyzed through calculations and simulations. By minimizing the metal area and integrating lumped/distributed inductors, we effectively reduced the cross-band scattering of the LB antenna without compromising its impedance bandwidth. The performance of this innovative array was validated through simulation, fabrication, and measurement. Results confirmed that the array operates efficiently within two important frequency ranges (0.85-0.98 GHz: GSM 850, GSM 900, UMTS 900, LTE 900, etc. and 1.4-2.7 GHz: IMT services, GSM 1800, UMTS 2100, LTE 2300, LTE 2500, LTE 2600, etc.). Additionally, the minimal interference between antennas operating in different bands makes this array particularly suitable for integrated vehicle-mounted base station applications, enhancing connectivity and performance in diverse environments.

REFERENCES

[1] Z. -X. Xia, K. W. Leung, P. Gu and R. Chen, "3-D-printed wideband high-efficiency dual-frequency antenna for vehicular communications," *IEEE Trans. Veh. Technol.*, vol. 71, DOI 10.1109/TVT.2022.3142015. no. 4, pp. 3457-3469, Apr 2022.

[2] H. A. Kayani, Q. Gueuning, N. Goreux, D. Vanhoenacker-Janvier, C. Oestges and C. Craeye, "Reconfigurable cellular base station antenna consisting of parasitic radiators," *IEEE Trans. Indus. Electr*., vol. 67, 10.1109/TIE.2019.2935991. no. 8, pp. 7083-7093, Aug 2020

[3] W. Wang et al., "Compact quad-element vertically-polarized high-isolation wideband MIMO antenna for vehicular base station," *IEEE Trans. Veh. Technol*., vol. 69, DOI 10.1109/TVT.2020.3004647. no. 9, pp. 10000-10008, Sept 2020.

[4] Y. Xu et al, "A wideband dual-polarized base station antenna with heat dissipation function based on PIN structure," *IEEE Trans. Veh. Technol*., vol. 72, DOI 10.1109/TVT.2023.3270842. no. 9, pp. 11924-11934, Sept 2023.

[5] X. Liu et al, "Differentially fed dual-band base station antenna with multimode resonance and high selectivity for 5G applications," *IEEE Trans. Antennas Propag*., vol. 72, DOI 10.1109/TAP.2023.3322198. no. 1, pp. 256-266, Jan 2024.

[6] Z. Zheng, D. Li, X. Tan and Q. Chen, "A compact low-profile differential dual-polarized filtenna without an external filter circuit for vehicular communications," *IEEE Trans. Veh. Technol*., vol. 72, DOI 10.1109/TVT.2022.3230220. no. 5, pp. 5587-5596, May 2023.

[7] Y. Cao, S. Yan, J. Li and J. Chen, "A pillbox based dual circularly-polarized millimeter-wave multi-beam antenna for future vehicular radar applications," *IEEE Trans. Veh. Technol*., vol. 71, DOI 10.1109/TVT.2022.3162299. no. 7, pp. 7095-7103, Jul 2022.

[8] H. Li, Y. Cheng, L. Mei and L. Guo, "Frame integrated wideband dual-polarized arrays for Mm-wave/Sub 6-GHz mobile handsets and its user effects," *IEEE Trans. Veh. Technol*., vol. 69, DOI 10.1109/TVT.2023.3270842. no. 12, pp. 14330-14340, Dec 2020.

[9] D. Bu, S. -W. Qu and S. Yang, "Planar, ultra-wideband and dual-polarized phased array antenna for millimeter-Wave vehicular communication," *IEEE Trans. Veh. Technol*., vol. 73, DOI 10.1109/TVT.2024.3364251. no. 7, pp. 9972-9983, Jul 2024.

[10] S. Yang, L. Liang, W. Wang, Z. Fang and Y. Zheng, "Wideband gain enhancement of an AMC cavity-backed dual-polarized antenna," *IEEE Trans. Veh. Technol*., vol. 70, DOI 10.1109/TVT.2021.3119643. no. 12, pp. 12703-12712, Dec 2021.

[11] G. Zhao et al, "Dual-polarized antenna arrays based on non-uniform partial reflective decoupling layers for vehicular base station systems," *IEEE Trans. Veh. Technol*., vol. 73, DOI 10.1109/TVT.2023.3327919. no. 3, pp. 3051-3064, Mar 2024.

[12] X. Liu et al., "A compact dual-polarized filtering antenna with steep cut-off for base-station applications," *IEEE Trans. Antennas Propag*., vol. 70, DOI 10.1109/TAP.2022.3161280. no. 7, pp. 5941-5946, July 2022.

[13] X. Liu et al., "Wideband dual-polarized antenna with high selectivity for 5G Sub-6-GHz base station applications," *IEEE Trans. Antennas Propag*., vol. 72, DOI 10.1109/TAP.2023.3329700. no. 1, pp. 962-967, Jan 2024.

[14] S. Zhang, X. Chen and G. F. Pedersen, "Mutual coupling suppression with decoupling ground for massive MIMO antenna arrays," *IEEE Trans. Veh. Technol*., vol. 68, DOI 10.1109/TVT.2019.2923338. no. 8, pp. 7273-7282, Aug 2019.

[15] X. Chen et al., "Simultaneous decoupling and decorrelation scheme of MIMO arrays," *IEEE Trans. Veh. Technol*., vol. 71, DOI 10.1109/TVT.2021.3134180. no. 2, pp. 2164-2169, Feb 2022.

[16] G. -W. Yang and S. Zhang, "A dual-band shared-aperture antenna with wide-angle scanning capability for mobile system applications," *IEEE Trans. Veh. Technol*., vol. 70, DOI 10.1109/TVT.2021.3072556. no. 5, pp. 4088-4097, May 2021.

[17] L. Ge, Y. Wang, M. Du, W. Liu and Y. Zhao, "A dual-band dual-polarized base station antenna array with isolation enhancement," *IEEE Open J. Antennas Propag*., vol. 4, DOI 10.1109/OJAP.2023.3309297. pp. 871-877, 2023.

[18] D. Yang, H. Zhai, C. Guo and C. Ma, "A novel differentially fed dual-polarized filtering magneto-electric dipole antenna for 5G base station applications," *IEEE Trans. Antennas Propag*., vol. 70, DOI 10.1109/TAP.2022.3161540. no. 7, pp. 5373-5382, July 2022.

[19] L. -H. Wen, S. Gao, Q. Luo, B. Sanz-Izquierdo, X. Ren and J. Wu, "Wideband differentially fed dual-polarized antenna by using three-strip transmission lines," *IEEE Trans. Antennas Propag*., vol. 69, DOI 10.1109/TAP.2020.3044629. no. 7, pp. 4172-4177, July 2021.

[20] J. Soric, Y. Ra'di, D. Farfan, and A. Alù, "Radio-transparent dipole antenna based on a metasurface cloak," *Nature Commun*., vol. 13, DOI 10.1038/s41467-022-28714-w. no. 1, pp. 1–8, Mar. 2022.

[21] D. He, Y. Chen and S. Yang, "A low-profile triple-band shared-aperture antenna array for 5G base station applications," *IEEE Trans. Antennas Propag*., vol. 70, DOI 10.1109/TAP.2021.3137486. no. 4, pp. 2732-2739, April 2022.

[22] Y. Zhu, Y. Chen and S. Yang, "Decoupling and low-profile design of dual-band dual-polarized base station antennas using frequency-selective surface," *IEEE Trans. Antennas Propag*., vol. 67, DOI 10.1109/TAP.2019.2916730. no. 8, pp. 5272-5281, Aug. 2019.

[23] H. -H. Sun, C. Ding, H. Zhu, B. Jones and Y. J. Guo, "Suppression of cross-band scattering in multiband antenna arrays," *IEEE Trans. Antennas Propag.,* vol. 67, DOI 10.1109/TAP.2019.2891707. no. 4, pp. 2379-2389, April 2019.

[24] H.-H. Sun, H. Zhu, C. Ding, B. Jones and Y. J. Guo, "Scattering suppression in a 4G and 5G base station antenna array using spiral chokes," *IEEE Antennas Wireless Propag. Lett.,* vol. 19, DOI 10.1109/LAWP.2020.3019930. no. 10, pp. 1818-1822, Oct. 2020.

[25] J. H. Zhai, Y. F. Cao, Q. Xue and W. Che, "Cross-band decoupling method for dual-band aperture-shared antenna array using metasurfaces," *IEEE Trans. Antennas Propag*., vol. 72, DOI 10.1109/TAP.2023.3344212. no. 2, pp. 2001-2006, Feb. 2024.

[26] H. Li, J. Xu, Y. Nan, Q. Chen and C. Zhou, "Low profile dual-band shared-aperture base station antennas based on FSS radiators," *IEEE Antennas Wireless Propag. Lett.,* vol. 23, DOI 10.1109/LAWP.2024.3372529. no. 6, pp. 1894-1898, Jun 2024

[27] Y. -S. Wu, Q. -X. Chu and H. -Y. Huang, "Electromagnetic transparent antenna with slot-loaded patch dipoles in dual-band array," *IEEE Trans. Antennas Propag*., vol. 70, DOI 10.1109/TAP.2022.3164194. no. 9, pp. 7989-7998, Sept. 2022.

[28] Y. He, W. Huang, Z. He, L. Zhang, X. Gao and Z. Zeng, "A novel cross-band decoupled shared-aperture base station antenna array unit for 5G mobile communications," *IEEE Open J. Antennas Propag*., vol. 3, DOI 10.1109/OJAP.2022.3173159. pp. 583-593, 2022.

[29] X. Lu, Y. Chen, S. Guo and S. Yang, "An electromagnetic-transparent cascade comb dipole antenna for multi-band shared-aperture base station antenna array," *IEEE Trans. Antennas Propag*., vol. 70, DOI 10.1109/TAP.2021.3137511. no. 4, pp. 2750-2759, April 2022.

[30] X. Liu et al., "A mutual-coupling-suppressed dual-band dual-polarized base station antenna using multiple folded-dipole antenna," *IEEE Trans. Antennas Propag.,* vol. 70, DOI 10.1109/TAP.2022.3209177. no. 12, pp. 11582-11594, Dec. 2022.

[31] R. Lampe, "Design formulas for an asymmetric coplanar strip folded dipole," *IEEE Trans. Antennas Propag*., vol. 33, DOI 10.1109/TAP.1985.1143698. no. 9, pp. 1028-1031, Sept 1985.

[32] E. Jordan and K. Balmain, *Electromagnetic Waves and Radiating Systems*. New York: Prentice-Hall, 1950 (first edition), 1968 (second edition).

[33] C. A. Balanis, *Antenna Theory: Analysis and Design*, 3rd ed. Hoboken, NJ, USA: Wiley, 2005.

[34] X. Liu, B. Sanz-Izquierdo, S. Gao, L. Wen and X. -X. Yang, "Wideband Dual-Polarized Filtering Antenna for Base Station Applications," *IEEE Antennas Wireless Propag. Lett*., doi: 10.1109/LAWP.2024.3364401.

[35] D. M. Pozar, Microwave Engineering, 3rd ed. New York, NY, USA: Wiley, 2005.

[36] S. J. Yang, R. Ma and X. Y. Zhang, "Self-decoupled dual-band dual-polarized aperture-shared antenna array," *IEEE Trans. Antennas Propag*., vol. 70, DOI 10.1109/TAP.2021.3137531. no. 6, pp. 4890-4895, June 2022.

[37] S. J. Yang and X. Y. Zhang, "Frequency selective surface-based dual-band dual-polarized high-gain antenna," *IEEE Trans. Antennas Propag*., vol. 70, DOI 10.1109/TAP.2021.3111222. no. 3, pp. 1663-1671, March 2022.

[38] Y. He, C. Ding, C. Chang, G. Wei and Y. J. Guo, "A bowl-shaped filtering antenna with wideband cross-band scattering mitigation for dual-band base stations," *IEEE Trans. Antennas Propag*., vol. 72, DOI 10.1109/TAP.2024.3390563. no. 8, pp. 6723-6728, Aug 2024.

Xuekang Liu (Member, IEEE) received the M.S. degree (Hons.) in electromagnetic field and microwave technology from Xidian University, Xi'an, China, in 2020, and the Ph.D. degree in engineering from the University of Kent, Canterbury, U.K., in 2024. He is a Research Associate with the School of Engineering, Lancaster University. His research interests include multiband arrays, transmitarrays, filtering antennas, RF systems, and MIMO antennas.

Dr. Liu was a recipient of the Best Student Paper Award at the 17th International Workshop on Antenna Technology (iWAT 2022), Dublin, and the Outstanding Academic Achievement for his M.S. program. He received the Young Scientist Award from the International Union of Radio Science (URSI) Member Committee, Germany, in 2022.

He actively contributes as a reviewer for more than ten prestigious international journals and conferences, including IEEE Transactions on Antennas and Propagation, IEEE Transactions on Instrumentation and Measurement, IEEE Antennas and Wireless Propagation Letters, and Nature Scientific Reports.

Benito Sanz-Izquierdo (Member, IEEE) received the B.Sc. degree from ULPGC, Spain, and the M.Sc. and Ph.D. degrees from the University of Kent, U.K.

He was Research Associate with the School of Engineering, University of Kent, in 2013, became a Lecturer in electronic systems, and a Senior Lecturer, in 2018. In 2012, he worked for Harada Industries Ltd., where he developed novel antennas for the automotive industry. His research has been funded through a variety of sources, such as the UK EPSRC, the Royal Academy of Engineering, and the Royal Society. His research interests include multiband antennas, wearable electronics, additive manufacturing (3D printing), substrate integrated waveguides components, metamaterials, electromagnetic band-gap structures, frequency selective surfaces, and reconfigurable devices. He has received awards and recognition for his work on wearable antennas (mention in the House of Lords and the IEEE IWAT Best Paper Award), frequency selective surfaces (best paper at an IET Workshop on Aerospace Applications Award), and reconfigurable antennas (2017 CST University Publication Award for an IEEE TRANSACTIONS Article) amongst others.

Steven Gao (M'01-SM'16-F'19) received the PhD from Shanghai University, China. He is a Professor at The Chinese University of Hong Kong (CUHK), Hong Kong, where he is also the Director of Center for intelligent Electromagnetic Systems. Prior to joining CUHK, he was a Professor and Chair of RF and Microwave Engineering at the University of Kent (UKC), UK during 2013-2022, and became an Honorary Professor at UKC since 2022. His research covers smart antennas, phased arrays, MIMO, reconfigurable antennas, broadband/multiband antennas, satellite antennas and wireless systems. He co-authored/co-edited 3 books, over 500 papers and 20 patents.

He is a Fellow of IEEE, and the Editor-in-Chief for *IEEE Antennas and Wireless Propagation Letters* and was a Distinguished Lecturer of IEEE Antennas and Propagation Society (2014-2016). He was the UK's Representative in European Association on Antennas and Propagation (EurAAP) during 2021-2022, and an Invited or Keynote Speaker at many international conferences (APMC 2024, IWOP 2024…).

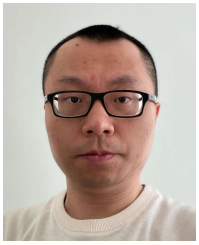

Qi Luo (Senior Member, IEEE) received the M.Sc. degree (Hons.) from the University of Sheffield, Sheffield, U.K., in 2006 and the Ph.D. degree (Hons.) from the University of Porto, Porto, Portugal, in 2012. From 2012 to 2013, he was a Research Fellow with the Surrey Space Center, Guildford, U.K. From 2013 to 2020, he was a Research Fellow with the School of Engineering and Digital Arts, University of Kent, Canterbury, U.K. He is a Reader in RF Engineering with the School of Physics, Engineering and Computer Science, University of Hertfordshire, Hatfield, U.K. His research interests include smart antennas, circularly polarized antennas, reconfigurable intelligent surfaces, metasurfaces, reflectarray, transmitarray, multiband microstrip antennas, and electrically small antenna designs.

Lu Zhang is currently a Lecturer in the Department of Computer Science at Swansea University. She received her B.Eng. in Electronic and Information Engineering from Xidian University, China, in 2016, and her M.Sc. (with distinction) in Mobile Communications from Loughborough University, UK, in 2018, where she was awarded the Clarke-Griffiths Best Student Prize. She completed her Ph.D. at Loughborough University in 2022.

Before joining Swansea University, she was a Research Fellow in Cyber Systems Engineering at the University of Warwick. Her research interests span deep learning and

adversarial learning, with a strong emphasis on their applications in wireless communications and cybersecurity.

Lehu Wen (Senior Member, IEEE) received Ph.D. degree in Electronic Engineering from the University of Kent, Canterbury, U.K., in 2020.

From 11/2020, he was a Research Fellow with the School of Engineering, University of Kent, Canterbury, UK. From 03/2023, he was a Research Fellow with the Department of Electronic and Electrical Engineering, University College London, UK. He is currently a Lecturer with the Department of Electronic and Electrical Engineering, Brunel University London, UK from 11/2023. His research interests include wideband Reflectarray, Transmitarray, dual-polarized antennas, circularly polarized antennas, tightly coupled array antennas, and mobile terminal antennas.

He received the Best Student Paper Award in ISAP2019, 1/10 Best Conference Paper in iWAT 2022, Best Paper Award (Flash Competition) in IEEE MTTS IWS2023. He was invited for talks on dual-polarized antennas in CAMA 2021 and APMC 2020. He was a Track Chair in IEEE ISAP 2022 and a Session Chair in EMW 2021. He served as the Track Chair in IEEE International Symposium on Antennas and Propagation 2022 and 2023. He was the Lead Guest Chair for Special Cluster of "Recent Advances in Filtering Antennas and Arrays" in IEEE Antennas and Wireless Propagation Letters, 2023. He serves as a regular Reviewer for journals of IEEE Transactions on Antennas and Propagation, IEEE Antennas and Wireless Propagation Letters, International Journal of RF and Microwave Computer-Aided Engineering, etc. He was an Exceptional Reviewer of IEEE Transactions on Antennas and Propagation in 2021-2023.

Xue-Xia Yang (Senior Member, IEEE) received the B.S. and M.S. degrees from Lanzhou University, Lanzhou, China, in 1991 and 1994, respectively, and the Ph.D. degree in electromagnetic field and microwave technology from Shanghai University, Shanghai, China, in 2001. From 1994 to 1998, she was a teaching assistant and a lecturer in Lanzhou University, China. From 2001 to 2008, she was a lecture and an associate professor in Shanghai University, China. She is currently a professor and the Head of the Antennas and Microwave R&D Center at Shanghai University. She has authored or coauthored over 300 technical journal and conference papers. She is also a frequent reviewer for over 10 scientific journals. Her research interests include antennas theory and technology, metasurface for antennas and microwave circuits, computational electromagnetics, and microwave power transmission. She is now the senior member of IEEE, the Committee of Antenna Society of China Electronics Institute, the Committee of Microwave Society of China Electronics Institute She is now an associate editor for *IEEE Antennas and Wireless Propagation Letters*, *Radio Science*, *Chinese Journal of Electronics*, etc.

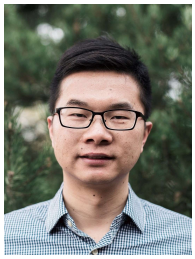

Lei Wang (Senior Member, IEEE) received the Ph.D. degree in electromagnetic field and microwave technology from the Southeast University, Nanjing, China in 2015. From 2014 to 2016, he was a Research Fellow in the Swiss Federal Institute of Technology (EPFL) in Lausanne, Switzerland. From 2016 to 2017, he was a Postdoc in the KTH Royal Institute of Technology in Stockholm, Sweden. From 2017 to 2020, he was an Alexander von Humboldt fellow in the Hamburg University of Technology in Hamburg, Germany. From 2020 to 2023, he was an Assistant Professor in the Heriot-Watt University in Edinburgh, United Kingdom. Since 2024, he is an Associate Professor (Senior Lecturer) in the Lancaster University in Lancaster, United Kingdom. His research includes antenna theory and applications, active electronically scanning arrays, integrated antennas and arrays, substrate-integrated waveguide antennas, leaky-wave antennas, wireless power transfer, and wireless propagations.

He has published more than 100 peer-review papers, book chapters, in addition to UK&US patents. He is the awardee of the National PhD Scholarship in China (2014), the Swiss Government Excellence Scholarship (2014), the Alexander von Humboldt fellowship (2016), Principal Investigator grant from German Research Foundation (DFG) (2020), the British Royal Society research grant (2022), the UK EPSRC international collaboration grant (2023) and the Innovate UK grants (2024, 2025). Moreover, he received the Best Poster Award in iWAT-2018, the Best Paper Award in UCET-2020, and the Best Antenna Paper Award in EuCAP-2023. He also supervised students winning the Honourable Mentioned Best Student Paper Award in APS-2021, the Best Student Paper Award in UCMMT-2022, and the Second Place Winner in IWS-2023.